RSC Advances

ROYAL SOCIETY OF CHEMISTRY

www.rsc.org/advances

RSC Advances

PAPER

Facile, low-cost, and scalable fabrication of particle size and pore structure tuneable monodisperse mesoporous silica nanospheres as supports for advanced solid acid catalysts†

Received 00th January 20xx,
Accepted 00th January 20xx

DOI: 10.1039/x0xx00000x

www.rsc.org/

Zhongkui Zhao*[a], Xianhui Wang[a], Yanhua Jiao[b], Boyuan Miao[a], Xinwen Guo[a] and Guiru Wang[a]

Monodisperse mesoporous silica nanospheres (MSN) have been emerging as one of the new fronties in materials science and nanotechnology because of their potential medical and biological applications as well as heterogeneous catalysis. Although the synthesis of MSN with various morphologies and sphere size has been reported, the synthesis of MSN with monodisperse control below 200 nm by a facile, scalable and low-cost method with high tetraethylorthosilicate (TEOS) concentration still remains a challenge. Herein, this goal was achieved by a templating hydrothermal technique using cetyltrimethylammonium bromide (CTAB) as the templating surfactant and low-cost urea as mineralizing agent. The mesoporous feature and diameter of nanosphere of MSN can be efficiently adjusted. The high volume efficiency by using high TEOS concentration as Si sources and the low production cost by using urea as mineralizing agent for synthesizing MSN allow this novel technique to have great potential for industrial production. Furthermore, the advanced solid acid catalysts with superior catalytic activity and stability were prepared by supporting phosphotungstic acid (PTA) on MSN, ascribed to the high PTA dispersity and facilitated mass transfer by the short mesoporous channels in comparison with traditional mesoporous silica like MCM-41. This work presents an alternative method for overcoming low stability issue, a bottleneck problem for the industrial application of solid acid catalysts.

1. Introduction

Since the discovery of MCM-41 in 1992 by Exxon Mobil Corporation, considerable progress has been made in the past decade in the synthesis of mesoporous materials with defined topology and morphology.[1] The synthesis of monodisperse mesoporous silica nanospheres (MSNs) has attracted special attention owing to their potential applications in drug delivery, cell imaging, separation, heterogeneous catalysis, adsorption of pollutants and so forth.[2] Chemical stability, homogeneous pore architecture, non-poison and recovery from colloidal solutions are required for some industrial applications of MSNs.[3]

Soft-templating technique is one of the best and easiest methods to synthesize MSNs because there is little aggregation, involving a well-defined pore structure, uniform morphologies, and particle size control. From references,[3a,3b] the polymorphic and polydispersed MSNs are produced under kinetic control using dilution and acid quenching. It has been found that the growth inhibitor additives, such as a triblock copolymer (F127),[3c] triethanol amines ($TEAH_3$),[4] and functional organosilanes,[5] improve the process, resulting in better particle size control. Without the addition of any additives, control of pore size and structure is still challenging.[6] Several groups have synthesized MSNs using microemulsion media.[7] However, these structures are either too large (>200 nm) for application in life sciences or too complex to be produced at a large scale.[8] Therefore, the development of a facile method for the production of MSNs with tunable porosity and particle size, particularly <200 nm, is highly desirable.

It was previously reported that the nanospherical mesoporous silica with an average size of 110 nm was produced,[9] but the extremely low TEOS concentration is indispensible. This would lower the volume efficiency of this technique, which depressed the scalable application of this method. Recently, a great breakthrough has been made on this issue, and the facile large-scale synthesis of MSNs with sphere diameter less than 200 nm at a high TEOS concentration by using a templating sol-gel technique.[8] However, the organic amines are required to be performed as the mineralizing agent. The use of relatively high cost and poison organic amines as mineralizing agent is contrary to the sustainable chemistry, besides the high production cost, which limits the large scale applications. It is highly attractive to develop a facile and sustainable low-cost scalable method to synthesize monodisperse MSNs with tunable particle size and pore structure.

Herein, a facile, low-cost and scalable approach is presented for synthesizing monodisperse MSNs with tuneable

[a] State Key Laboratory of Fine Chemicals, Department of Catalysis Chemistry and Engineering, School of Chemical Engineering, Dalian University of Technology, Dalian 116024, P.R. China. E-mail: zkzhao@dlut.edu.cn; Fax:+86-411-84986354.
[b] College of Material Chemistry and Chemical Engineering, Hangzhou Normal University, Hangzhou 310036, P. R. China.

†Electronic supplementary information (ESI) available. See DOI: 10.1039/cxraxxxxx.

particle size and pore structure through a templating hydrothermal technique using CTAB as the templating surfactant and urea as the mineralizing agent from the Advanced catalytic Materials Research Group, DLUT. The particle size and pore structure can be adjusted by changing the urea concentration. The application properties of the MSNs were measured in heterogeneous catalysis. The as-synthesized MSNs with appropriate pore structure and particle size could be employed as an excellent support to prepare advanced solid acid catalysts. The catalytic stability is still a bottleneck problem for the industrial application of solid acid catalysts, the developed supported PTA catalyst on MSN (PTA/MSN) demonstrates much superior catalytic activity and stability for the alkenylation of *p*-xylene with phenylacetylene, a model reaction for clean and atomic economic synthesis of alpha-arylstyrenes,[10] as well as outstanding catalytic efficieny for diverse reactions like esterification, alkylation, and benzylation. The improvement of coke-resistent stability through shortening the length of mesopores is sapiential strategy to solve the bottleneck problems of solid acid catalysts for their industrial applications. Moreover, this work presents a practical technique for synthesizing monodisperse MSNs with less than 200 nm of particle size and the tuneable pore structure, which can act as promising candidate for drug delivery, cell imaging, separation, heterogeneous catalysis, adsorption of pollutants and so forth.

Experimental section

Synthesis of MSNs

The synthesis was performed under mild conditions with a typical composition of 1.0TEOS: 0.064CTAB: *x*urea: 300 H_2O at a molar basis, where *x* (urea/TEOS) varied from 0.01 to 8.0. In a typical synthesis of MSN, 0.816 g cetyltrimethylammonium Bromide (CTAB), the required amount of urea based on *x* values were dissolved in 200 g H_2O and stirred for 1 hour, and then 7.3 g of tetraethylorthosilicate (TEOS) was added dropwise into the above solution. The mixture was stirred at 80 ^oC for 2 hours. After that the milky liquid was injected into Teflon-lined autoclave and heated at 100 ^oC for 20-60 hours. The obtained solid product was recovered, washed, and then dried at 105 ^oC for 20 h. The final MSNs were obtained by calcining the above samples at 550 ^oC for 6 h, and labelled as MSN-0.01, MSN-0.025, MSN-0.1, MSN-2.5, and MSN-8, respectively, based on the diverse *x* values for the mother liquor composition.

Synthesis of PTA/MSN-x solid acid catalysts

According to our previously reported vacuum assisted wet impregnation with heating method (IMPVH), the supported PTA catalysts on MSN-*x* were synthesized. Typically, the as-synthesized MSN-*x* power was sieved into 20-60 mesh particles after tableting. The PTA was supported on MSN-*x* supports via IMPVH method. The method exploited in our case was carried out by impregnating MSN-*x* (1.0 g) with an aqueous solution of PTA (the concentrations is 0.36 g ml^{-1}) in a vacuum environment with heating at 128 ^oC. Then the impregnated samples were dried at 105 ^oC in air overnight, followed by calcinations in air at 300 ^oC for 3 hours, and the PTA/MSN-*x* catalysts with a loading of 25 wt % were obtained.

Characterization of Samples

X-ray diffraction (XRD) profiles were collected from 10 to 80° at a step width of 0.02° using Rigaku Automatic X-ray Diffractometer (D/Max 2400) equipped with a CuKa source (λ= 1.5406 Å). Nitrogen adsorption and desorption isotherms were determined on a Micromeritics apparatus of a model ASAP-2050 system at -196 ^oC. The specific surface areas were calculated by the BET method, and the pore size distributions were calculated from an adsorption branch of the isotherm by the BJH model. Transmission electron microscopy (TEM) images were obtained by using a Tecnai F30 HRTEM instrument (FEI Corp.) at an acceleration voltage of 300 kV. FT-IR spectroscopy characterization of catalysts was performed at 150 ^oC under ultrahigh vacuum using a Bruker EQUINOX55 infrared spectrometer. NH_3-TPD measurements were performed to characterize the acidity of the samples. After pretreatment of 50 mg samples in Ar (up to 300 ^oC with a ramp rate of 10 ^oC min^{-1}, and then kept for 0.5 h under 30 ml min^{-1} Ar flow), the samples were saturated with ammonia (10% NH_3–90% Ar) at 10 ^oC via the pulse injection of ammonia in an Ar stream. The desorptions steps were carried out from 100 and 700 ^oC at a heating rate of 10 ^oC min^{-1} and with an Ar flow of 30 ml min^{-1}. The NH_3-TPD profiles were obtained via monitoring the desorbed ammonia with a thermal conductivity detector.

Catalytic Performance Measurement

The experiments on the alkenylation of aromatics with phenylacetylene were performed in a stainless steel fixed-bed continuous-flow reactor. A sample of 0.8 g PTA/MSN catalyst with 20-60 mesh was loaded into the reactor for all the reaction tests, and the remaining space of the reactor tube was filled with 20-60 mesh quartz granules. Before the introduction of feedstock, the catalyst was preactivated for 1 h online in N_2 flow. The liquid stream was introduced into the fixed-bed reactor by a syringe pump. N2 (99.999% purity) was used to maintain system pressure. In all cases, a time on stream of 8 h was used. The PTA/MCM-41 and PTA/NSN were aslo measured for comparison. Quantitative analysis of the collected products was performed on a FULI 9790 II GC equipped with an HP-5 column, 30 m × 0.32 mm×0.25μm, and an FID detector. The phenylacetylene conversion was calculated by weight percent of the consumed phenylacetylene in the total phenylacetylene amount in the feed; the selectivity to alpha-arylstyrene was calculated by weight percent of desired alpha-arylstyrene in total products. The reaction rate was calculated on the basis of molar amount transformed reactants per mole of acidic sites per hour or based on the transformed reactants per gram catalyst per hour.

Results and discussion

Synthesis and Characterization of Particle Size and Pore Structure Tunable MSNs

The synthesis of MSMs was performed with a typical mother liquor composition of $1.0SiO_2$:0.06CTAB:*x*Urea:$300H_2O$ at a molar basis, where *x* (molar ratio of urea to TEOS) vaired from 0.01 to 8. Typically, 0.816 g of CTAB and the required amount of urea based on *x* value was dissolved into 200 ml deioned water, and then the 7.3 g of TEOS was added dropwise into the above solution with stirring. The resulting mixture was transferred into Teflon-lined autoclave and heated at 105 ^oC for 48 hours. The obtained solid product was recovered, washed, and then dried at 105 ^oC for 20 h. The final MSNs were obtianed by calcining the above samples at 550 ^oC for 6 h, and labelled as MSN-0.01, MSN-0.025, MSN-0.1, MSN-2.5, and MSN-8, respectively, based on the diverse *x* values for the mother liquor composition. The detailed synthesis process can be seen in the experimental section.

Fig. 1 presents the typical TEM images of the as-synthesized MSN-*x*, and their particle size distribution is depicted in Fig. S1 and Table 1. Fig. 1 clearly demonstrates that the monodisperse spherical mesoporous silica particles have successfully synthesized by the developed templating hydrothermal method using CTAB as templating surfactant and urea as mineralizing agent. From Fig. S1, 1, and Table 1, it can be found that the particle size is strong dependent on the

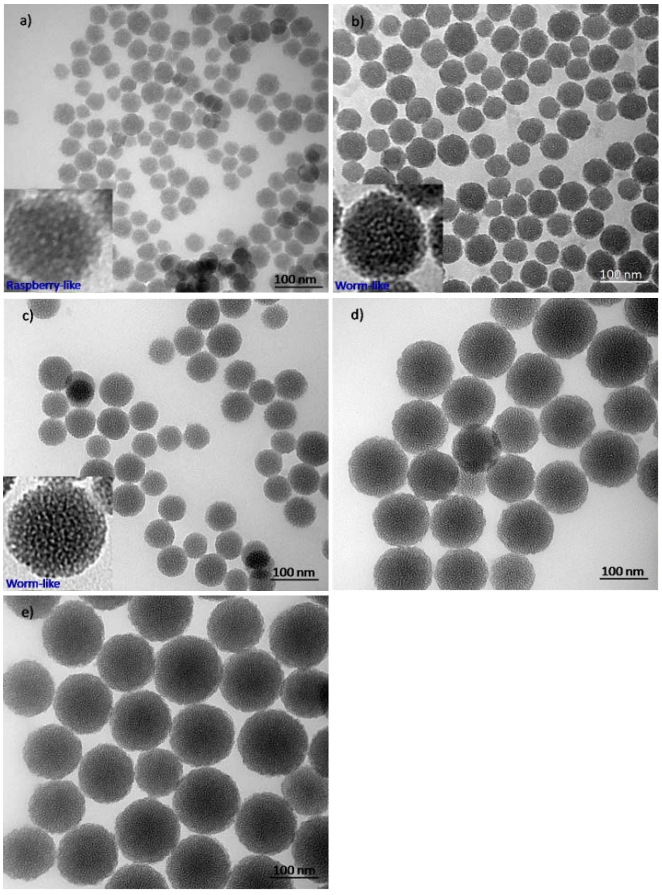

Fig. 1. TEM images of the as-synthesized MSN-x with diverse molar ratios of urea (mineralizing agent) to TEOS (silica source). a) x=0.01, b) x=0.025, c) x=0.1, d) x=2.5, and e) x=8. The insets in the Fig. 1a and 1b are the magnified regions.

molar ratio of urea to TEOS, and average size increased from 37 to 130 nm as the *x* value rose from 0.01 to 0.1. The lower molar ratio of urea to TEOS (lower PH) results in smaller particle size, and even the MSNs with less than 100 nm of particle size can also be achived while the 0.01-0.1 of molar ratio of urea to TEOS is used. The higher urea concentration can produce more OH^-, which enhances the hydrolysis rate of TEOS. As a consequence, the more self-assembled silicate micelles quickly form, and the MSNs particles with larger size can be resulted, which is in consistent with the reported results.[8,11] More interestingly, the difference in urea concentration can change the pore channel morphology. From Fig. 1, the raspberry-like pores can be formed while the 0.01 of molar ratio of urea to TEOS was used; whereas the worm-like pore channels can be formed while the ratio was not less than 0.025. Scheme 1 demonstrates the schematic illustration for the formation of the diverse pore channels led by the change of molar ratio of urea to TEOS. From references,[8,12] the spherical mesoporous silica is formed through two steps: one is the fomation of silicated mecelles, the other is the aggregation of the as-formed silicated micelles. Using lower urea concentration, the Br^- counterions of CTAB surfactant micelles are slowly substituted by the formed silicate. Subsequently, the MSNs with spherical (raspberry-like) pore channels is synthesized through the aggregation of the spherical silicated micelles. Such a rapberry-like pore morphology was previously reported only in polymorphic and polydispersed systems obtained by using both dilution and PH quenching. In this work, the use of the urea as mineralizing agent and the low urea concentration might provide thus reaction environment, and therefore the MSNs with raspberry-like pore morphology have been successfully synthesized. If the urea concentration is increased to a certain value, i.e. 0.025 of molar ratio of urea to TEOS (the total amount of water is fixed, the larger ratio means the higher urea concentration), the large amount of silicate is quickly formed, which can wrap the several surfactant micelles and then the worm-like silicated micelles are formed. Then worm-like silicated micelles-containing aggregates are produced. After the subsequent calcination process, the MSNs with worm-like mesopores were synthesized.

Nitrogen adsorption-desorption isotherms of the as-synthesized MSNs are presented in Fig. 2a. All of the isotherms are of type IV according to IUPAC classification and exhibit H1 hysteresis with a featured capillary condensation in the mesopores, indicating the presence of mesopores.[13] It's interesting that the isotherms present two clear capillary condensation steps: one is at 0.15-0.50 of a lower relative pressure (p/p_0) and the other is at 0.8-1.0 of a higher relative pressure region, implying the pore feature of MSNs with bimodal mesopores.[14] The bimodal "mesopores"are also confirmed by the BJH adsorption pore szie distribution. As can be seen from Fig. 2b, the as-synthesized MSNs contain two types of pores with small mesopores (the center of the pore distribution from the adsorption branch is 2.8 nm, also can be clearly observed in the TEM images shown in Fig. 1) and large

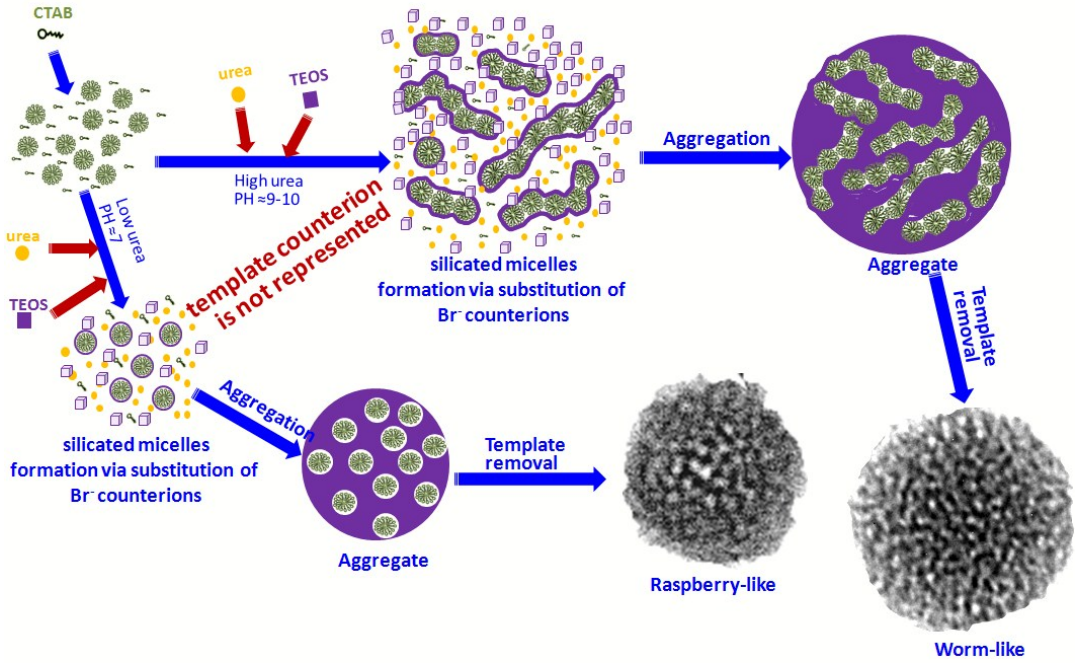

Scheme 1. Schematic illustration for the formation of monodisperse mesoporous silica nanospheres (MSN) with diverse pore structures depending on the molar ratio of urea to TEOS.

mesopores (25-250 nm, based on IUPAC classification, the latter may be assigned to larger mesopores or large pores). The smaller mesopores are thought to be generated by the removal of templating surfactant, whereas the larger mespores or larger pore channels can be originated from the accumulation of MSNs. The Brunauer-Emmett-Teller surface area (S_{BET}), Barrett-Joyner-Halenda pore volume (V_{BJH}), micropore surface area by T-plot method (S_{mic}), micropore pore volume by T-plot method (V_{mic}), and the BJH pore diameters (D_{BJH}) from the adsorption branch of isotherms the series of MSNs (MSN-*x*, *x*=0.01, 0.025, 0.1, 2.5, 8) are summarized in Table 1. The specific surface area of MSNs increases with the increase in urea concentration. However, the micropores appear while the molar ratio of urea to TEOS is not less than 0.1, which can be confirmed by the sharp increased adsorbed amount with the increase in relative pressure (p/p_0) at lower p/p_0 region shown in Fig. 2a. But it is concluded that much more micropore come into reality as the concentration of urea increase. That may because under alkaline conditions (pH > 7.0), silicates with a high negatively-charged density can only assemble with the cationic surfactants through strong electrostatic interaction. The fast silica condensation and strong electrostatic interactions between silica and cationic surfactants induce the fast simultaneous assembling-growth of the silica-surfactant nuclei, which also leads to the increase in particle size of MSN-*x* with the increasing *x* value.[11] By deducting the micropore surface area, no obvious change in the left surface area can be observed as the *x* value increases. As the *x* value increases, no large change in BJH pore diameters generated from the removal of templating surfactant take places (it increases from

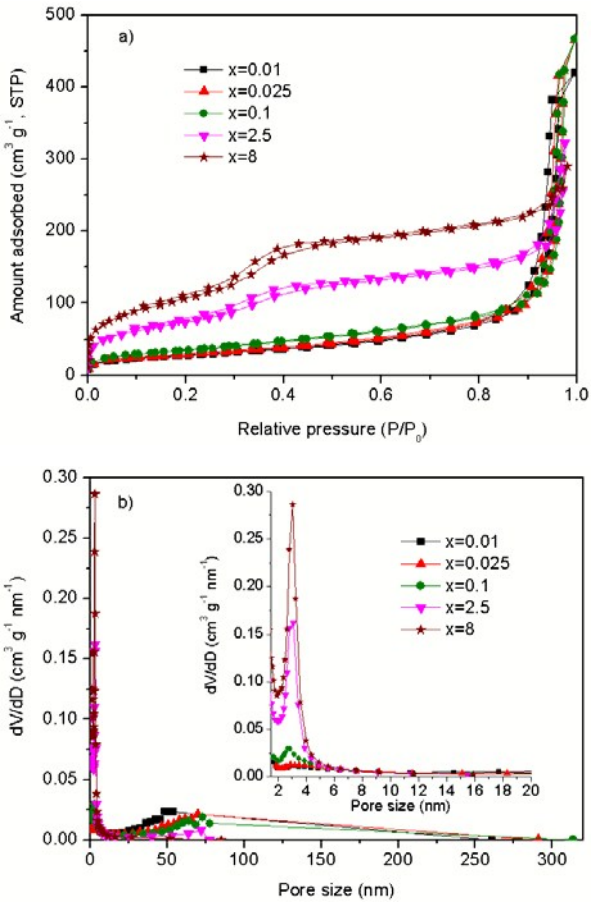

Fig. 2. N_2 adsorption-desorption isotherms (a) and the Barrett-Joyner-Halenda (BJH) pore size distribution from adsorption branch of the as-synthesized mesoporous silica nanosphere MSN-*x* with diverse *x* values.

Table 1 Textural properties of the as-prepared MSN-*x* samples.

Sample	S_{BET} [a] [$m^2 g^{-1}$]	V_{BJH} [b] [$cm^3 g^{-1}$]	S_{mic} [c] [$m^2 g^{-1}$]	V_{mic} [d] [$cm^3 g^{-1}$]	D_{BJH} [e] [nm]	*PSD* [nm] [f]
MSN-0.01	98	0.68	0	0	2.8/35	37±11
MSN-0.025	104	0.75	0	0	2.8/45	53±9
MSN-0.1	125	0.75	24	0.02	2.8/50	63±8
MSN-2.5	273	0.54	173	0.13	2.9/70	113±4
MSN-8	395	0.49	274	0.21	3.01/--	130±14

[a] denoted as the specific surface area. [b] denoted as the BJH pore volume from the adsorption branch. [c] denoted as micropore surface area by T-plot method. [d] denoted as micropore volume by t-plot method. [e] Denoted as is the center of the pore distribution from the adsorption branch. [f] Denoted as particle size distribution, obtained from TEM images shown in Fig. 1.

2.8 to 3.0 nm as the *x* rises from 0.01 to 8), whereas the pore diameter of the accumulated pore increases as the x value increases from 0.01 to 2.5. No accumulated pore can be observed as the 8 of molar ratio of urea to TEOS can be used. Moreover, the increase in urea concentration leads to a visible decrease in BJH pore volume. The textural features can affect the acidic properties of the supported PTA catalysts on MSN-*x*, besides affect the mass transfer for solid acid catalyzed transformations. As a consequence, they can affect the catalytic properties of PTA/MSN-*x*.

Catalytic Performance Measurement of the PTA/MSN-*x* Solid Acid Catalyst

Based on the above work, a series of MSNs with diverse particle sizes and pore structures have been successfully synthesized. In the synthesis process, the low-cost and non-poison urea was employed as mineralizing agent to replace the previously reported high-cost and poison organic amines like such as triethanolamine, 2-amino-2-(hydroxymethyl) propane-1,3-diol, and triethyleneamine. Moreover, from previous reports, the MSNs with less than 200 nm of particle size could be a promising candidate for diverse applications including heterogeneous catalysis, medical, and biological fields. Therefore, this novel technique developed in this work has more practical applications in industry.

The supported PTA solid acid catalysts on mesoporous supports have attracted great attention in diverse transformations owing their excellent catalytic performance.[15] Herein, we evaluated the application properties of MSNs in heterogeneous catalysis by employing them as supports to prepare the supported PTA solid acid catalysts for diverse transformations including alkenylation, esterification, alkylation, and benzylation reactions. Fig. 3 presents the typical TEM images of the supported PTA catalysts on diverse MSN-*x* (*x*=0.01, 0.025, 0.1, 2.5, 8). From Fig. 3, the similar morphology feature of the supported PTA catalysts on MSN to that of the supports shown in Fig. 1 can be observed, except for the existence of black dots assigned to PTA aggregate within the MSNs shown in Fig. 3d-f. Moreover, although the surface area of the MSNs supports increases with the increasing *x* value, the PTA dispersity decreases, and even the PTA aggregate can be clearly seen in the TEM images of the supported catalysts on MSN-2.5 and MSN-8 (Fig. 3d and e).

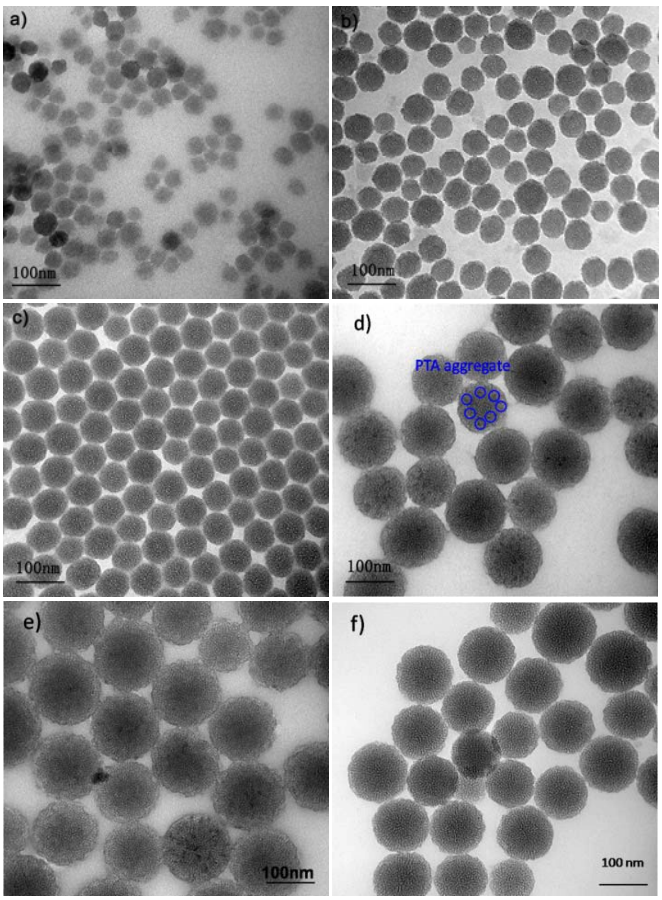

Fig. 3. TEM images of the supported PTA catalysts on the as-synthesized MSN-*x* silica nanospheres with different *x* values. a) PTA/MSN-0.01, b) PTA/MSN-0.025, c) PTA/MSN-0.1, d) PTA/MSN-2.5, e) PTA/MSN-8. The image of f) MSN-2.5 support is included for comparison.

Table 2 Textural properties of the supported PTA catalysts on the diverse MSN-*x* supports.

Sample	S_{BET} [a] [$m^2 g^{-1}$]	V_{BJH} [b] [$cm^3 g^{-1}$]	S_{mic} [c] [$m^2 g^{-1}$]	V_{mic} [d] [$cm^3 g^{-1}$]	D_{BJH} [e] [nm]	Acidity (mmol g^{-1})
PTA/MSN-0.01	124	0.79	0	0	2.8/35	0.37
PTA/MSN-0.025	91	0.72	0	0	2.8/70	0.25
PTA/MSN-0.1	58	0.50	0	0	2.8/70	0.24
PTA/MSN-2.5	98	0.40	41	0.03	2.8/90	0.22
PTA/MSN-8	179	0.29	118	0.08	2.8/--	0.21

[a] denoted as the specific surface area. [b] denoted as the BJH pore volume from the adsorption branch. [c] denoted as micropore surface area by T-plot method. [d] denoted as micropore volume by T-plot method. [e] Denoted as is the center of the pore distribution from the adsorption branch. [f] Denoted as particle size distribution, obtained from TEM images shown in Fig. 3.

The decreasing PTA dispersity can be ascribed to the decrease in BJH pore volumes of mesopores in the MSNs. Higher PTA dispersity would result in more acidic sites (Fig. S2 and Table 2).

The textural features of the PTA/MSN-*x* catalysts were characterized by N_2 adsorption-desorption analysis. Fig. S3 presents the N_2 adsorption-desorption isotherms of the PTA/MSN-*x* catalysts, and the textural features are summarized in Table 2. From Fig. S3 and Table 2, the PTA/MSN-*x* catalysts have the similar isotherms and pore size

distributions. By comparing the textures of MSN supports (Table 1) and the PTA/MSN-*x* catalysts (Table 2), it can be found that, except for the PTA/MSN-0.01 catalyst, the decreasing surface area and BJH pore volume can be observed. More interestingly, the decreases in surface area (S_{BET} and S_{mic}) and pore volume (V_{BJH} and V_{mic}) towards the samples with 0.1 to 8 of x values are quite dramatic. Combining the visible PTA aggregate on the supported PTA catalysts on MSNs with larger *x* value, it can be proposed that the above decrease in surface area and pore volume can be mainly ascribed to the block of pore channels, especially the block of micropores on the samples with 0.1-8 of *x* values. Moreover, towards the MSN-0.01 support and PTA/MSN-0.01 catalyst, the surface area and pore volume don't decrease but increase, might be ascribed to the formed pores from the dispersed PTA on the surface of the accumulated mesopores (35 nm), whereas the accumulated pores on the samples with 0.1-8 of x values are too large (larger than 50 nm) to form the mesopores. Moreover, From Fig. 2b, Fig. S3b, Table 1, and Table 2, the pore volume corresponding to accumulated pores after supporting PTA on MSNs supports, might be resulted from the block of PTA. From Table 1 and 2, the center of accumulated pores of PTA/MSNs is larger than that of MSNs, owing to the change of accumulate feature in the supporting PTA process.

The catalytic performance of PTA/MSN-*x* with diverse molar ratio of urea to TEOS for alkenylation of *p*-xylene with phenylacetylene, as a model reaction, was measured. The results are demonstrated in Fig. S4. The conversion of phenylacetylene decreases with the increasing *x* from 0.01 to 0.025, and reaches the maximum over the PTA/MSN-0.025. The decreasing conversion can be observed as the *x* value is further increased from 0.025 to 8. No visible change in selectivity towards alpha-arylstyrene can be observed as the *x* value rises from 0.01 to 8 (Fig. S4). The decreasing catalytic activity with the increase in x value from 0.025 to 8 can be ascribed to the increase in length of mesopores led by the larger particle size, besides the lowering acidic sites shown in Fig. S2 and Table 2. More interestingly, the PTA/MSN-0.01 demonstrates lower catalytic activity in comparison with PTA/MSN-0.025, although the former has more acidic sites and smaller particle size than the latter. This may be ascribed to the worse mass transfer over the PTA/MSN-0.01 catalyst than that over PTA/MSN-0.025 led by different pore channels morphologies. The raspberry-like mesopores in PTA/MSN-0.01 but worm-like ones in PTA/MSN-0.025 have been confirmed in Fig. 1 and 3. Therefore, we can safely say that the catalytic performance of the supported PTA catalysts on MSN-*x* supports is strongly dependent on the pore morphology, besides dependent on the acidic properties. It can be also concluded that the worm-like mesopores favor the catalytic reaction owing to more favorable mass transfer in comparison with the paspberry-like ones. The supported PTA catalyst on MSN-0.025 support with worm-like pore feature and smaller particle size exhibits the best catalytic performance among all of the PTA/MSN-*x* (*x*=0.01, 0.025, 0.1, 2.5, 8) catalysts.

Moreover, no clear peak on the low-angle XRD pattern of PTA/MSN-0.025 (Fig. S5) can be well-resolved, suggesting the mesopores of PTA/MSN-0.025 catalyst confirmed by TEM images and N_2 adsorption analysis are not well-ordered. However, the disordered feature of the mesopores doesn't depress the catalytic performance of PTA/MSN-0.025, which can be partially confirmed by the comparison of its catalytic performance with that of PTA/MCM-41 catalyst presented in Table 3. Under the same reaction conditions, the developed PTA/MSN-0.025 exhibits superior catalytic performance to PTA/MCM-41 catalyst. 99.4% and 83.7% conversion of phenylacetylene can be obtained over the PTA/MSN-0.025 and PTA/MCM-41, respectively. Furthermore, now that PTA/MSN-0.025 only has disordered mesopores, we also have a doubt that the small size of PTA/MSN-0.025 may be the reason for it exhibiting the outstanding catalytic performance, although this issue has been primarily confirmed by the instance that PTA/MSN-0.025 has a larger particle size but exhibits higher catalytic activity in comparison with PTA/MSN-0.01. We compared the catalytic performance of PTA/MSN-0.025 catalyst with supported PTA catalyst on the smaller silica nanospheres without mesopores (PTA/NSN). According to reference,[16] the monodisperse non-porous silica nanospheres with less than 15 nm of particle size (NSN) were synthesized. From Table 4, the NSN nanoparticle has much larger surface area than MSN (260 and 104 $m^2\ g^{-1}$ for NSN and MSN, respectively). The former doesn't have mesopores, and the much larger surface area of NSN than MSN is owing to the smaller silica particle size of NSN. From Table 3, PTA/NSN exhibited much lower catalytic activity than PTA/MSN-0.025, although PTA/NSN has much higher surface area (176 $m^2\ g^{-1}$) in comparison with PTA/MSN-0.025 (91 $m^2\ g^{-1}$). This presents an instance that the existence of the worm-like mesopores in the MSN-0.025, although they are disordered mesopores, significantly favors the catalytic reaction. Furthermore, the acidic properties of the supported PTA catalysts on MSN-0.025, MCM-41, and NSN (with the same PTA loading) were measured by NH_3-TPD (Fig. 4 and Table 4). The much higher surface area and larger pore volume of MCM-41 allows the PTA/MCM-41 catalyst to have 0.52 mmol g^{-1} of highest acidic concentration owing to the improved PTA dispersity confirmed by XRD analysis (Fig. S6), whereas the PTA/NSN has lowest acidic concentration owing to its non-porous feature (0.20 mmol g^{-1}). The developed PTA/MSN-0.025 demonstrates much high *TOF* (8.9 h^{-1}) for alkenylation reaction than the other two catalysts (3.6 and 5.6 h^{-1} over PTA/MCM-41 and PTA/NSN,

Table 3 Reaction result of the alkenylation of p-xylene with phenylacetylene over the supported PTA catalysts on the developed MSN-0.025, as well as on the traditional mesoporous silica MCM-41 and the non-porous silica nanosphere NSN.[a]

Catalyst	Con. (%)	Product distribution (%)				
		α-AS[b]	AP[c]	HP[d]	IS[e]	OL[f]
PTA/MCM-41	83.7	91.8	1.8	0.1	2.5	3.8
PTA/MSN-0.025	99.4	95.1	1.0	0.1	0.8	3.0
PTA/NSN	49.7	92.6	1.8	0.1	4.0	1.5

[a] Reaction conditions: catalyst 0.8 g, $n_{p\text{-}xy/Phen}$ 25:1, T_r 150 °C, P_s 1.0 MPa, *VHSV* 7.2 ml $h^{-1}\ g^{-1}$ cat; *TOS* 8 h. [b] denoted as α-arylstyrenes. [c] denoted as acetophenone. [d] denoted as hydrogenation products. [e] denoted as Isomers. [f] denoted as oligomers.

Table 4 Textural feature, average crystalline size of PTA, acidic properties, and turn of frequency (TOF) of the developed PTA/MSN-0.025 catalyst as well as PTA/MCM-41 and PTA/NSN catalysts with same PTA loading are included for comparison.

Sample	S_{BET} ($m^2\ g^{-1}$)	V_{total} ($cm^3\ g^{-1}$)	D_{BJH} (nm)	CS^a (nm)	Acidity (mmol g^{-1})	TOF^b (h^{-1})
PTA/MSN-0.025	91	0.7	2.7	16.7	0.25	8.9
MSN-0.025	104	0.7	2.7	--	--	--
PTA/MCM-41	519	0.6	2.9	15.8	0.52	3.6
MCM-41	1054	1.1	2.9	--	--	--
PTA/NSN	176	--	--	--	0.20	5.6
NSN	260	--	--	--	--	--

[a] Average crystalline size of PTA supported on diverse supports including the developed mesoporous silica nanosphere (MSN-0.025) and the traditional mesoporous silica (MCM-41) as well as the non-precious silica nanosphere (NSN). [b] Denoted as the mmol product per mmol of acidic sites. Reaction conditions: catalyst 0.8 g, $n_{p\text{-}xy/Phen}$ 25:1, T_r 150 °C, P_s 1.0 MPa, *VHSV* 7.2 ml h^{-1} g^{-1}cat; *TOS* 8 h.

respectively), although it has lowest surface area. This can be ascribed to their unique pore features. Although both PTA/MSN-0.025 and PTA/NSN have accumulated pores, the former has mesopores in nanospheres but the latter has no mesopores in silica nanosphere. This result presents a clear instance that the presence of disordered worm-like mesopores in PTA/MSN-0.025 plays an important role in catalyzing the alkenylation reaction. In comparison with PTA/MCM-41, the PTA/MSN-0.025 shows 2.5 times of much higher *TOF* for alkenylation, ascribed to their different mesopore features. Now that MCM-41 generally has several micrometers of particle size, the length of mesopores in MSN-0.025 is much shorter than the length of hexagonal ones in MCM-41. This could efficiently facilitate mass transfer by shortening diffusion distance in the alkenylation process over the PTA/MSN-0.025 solid acid catalyst in comparison with PTA/MCM-41. In comparison with the reported results, the developed PTA/MSN-0.025 catalyst demonstrates much better catalytic performance.[10,18]

Besides the improved activity over PTA/MSN-0.025 in comparison with PTA/MCM-41, the facilitating mass transfer

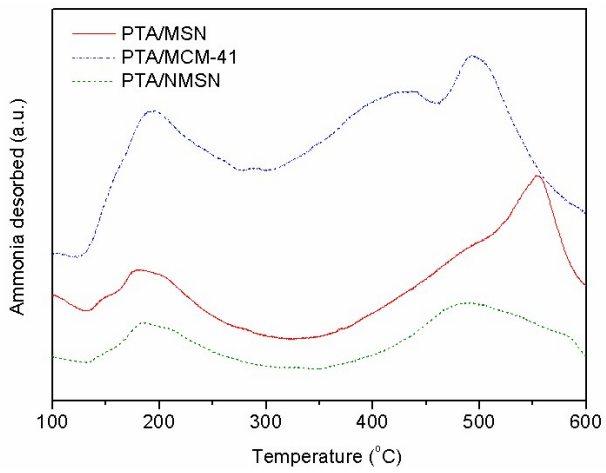

Fig. 4. NH_3-TPD profiles of the developed 25 wt.%PTA/MSN-0.025 catalyst, and the supported PTA caatlysts on MCM-41 and NMSN are included for comparison.

over PTA/MSN-0.025 can efficiently improve the catalytic stability. It is generally accepted that the depressed catalytic stability is the bottleneck problem for the application of solid acid catalysts in industry. The deactivation of solid acid catalyst mainly results from the coke deposition led by acid catalyzed polymerization. The too strong acidic sites and the long staying time of reactants or products can enhance this coke deposition process.[17] Especially for the direct alkenylation of aromatics with alkyne for producing alpha-arylstyrenes, the coke issue of solid acid catalyst is particularly acute owing to the tendency to polymerization of both reactant (alkyne) and the formed product (alpha-arylstyrenes).[10,18] If the formed alpha-arylstyrenes can't be timely removed through diffusion, the solid acid catalyst would suffer from serious deactivation by coke deposition. Besides the development of efficient methods such as alkaline earth and rare earth modification to eliminate the too strong acidic sites,[19] the intensification of mass transfer would be a sapiential strategy. It was previously reported from our ACM research group that,[10] the mesoporous solid acid demonstrated much better coke-resistent stability in comparison with zeolite owing to facilitated mass transfer. Although the enlargement of pore diameter from micropore to mesopore efficiently improves the stability of solid acid catalysts,[10,20] this kind of improvement is of a limited strategy owing to the poor hydrothermal stability and lower surface area led by too larger mesopore or the macropore.[21] Especially, towards the H_2O-including reaction systems, like esterification, dehydration, hydration, etc., the hydrothermal stability is also important issue. Therefore, the development of new strategy to enhance the diffusion is highly desirable.

The shortening of length of mesopore in the solid acid catalysts would be a sapiential strategy.[22] This strategy was examined by employing the alkenylation of *p*-xylene with phenylacetylene as a model reaction. From Fig. 5, the PTA/MSN-0.025 catalyst demonstrates much higher activity and stability along with time on stream. Scheme 2 illustrates the schematic for this enhancing effect. Owing to the stronger acidic sites of PTA/MSN-0.025 catalyst in comparison with PTA/MCM-41, the improvement in the stability by the suppressed coke formation doesn't come from a decrease in strong acidic sites. Owing to only 53 nm of average particle size, the worm-like mesopores in the MSN-0.025 is much shorter than the hexagonal mesopores in MCM-41 with several micrometers of particle size. The formed alpha-arylstyrenes could quickly leave from the solid acid catalysts before they would suffer from ploymerization process. As a result, the PTA/MSN-0.025 solid acid catalyst demonstrates superior coke-resistent stability in comparison with PTA/MCM-41. The presented approach by shorting length of mesopore of the mesoporous solid acid catalysts can be considered as a sapiential strategy for improving coke-resistent stability of solid acid catalysts. Moreover, the developed PTA/MSN-0.025 could be a promising solid acid catalyst for the production of alpha-arylstyrenes through direct alkenylation of diverse aromatics with alkynes.

Furthermore, besides for above alkenylation, the catalytic

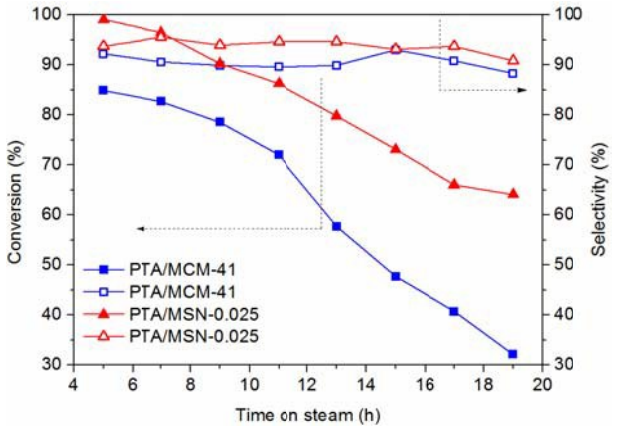

Fig. 5. A comparison between PTA/MSN-0.025 and PTA/MCM-41 on the catalytic stability for the alkenylation of *p*-xylene with phenylacetylene. Reaction conditions: catalyst 0.8 g; $n_{p\text{-}xy/Phen}$ 25:1; T_r 150 °C; P_s 1.0 MPa; VHSV 7.2 ml h^{-1} g^{-1}cat; TOS 8 h.

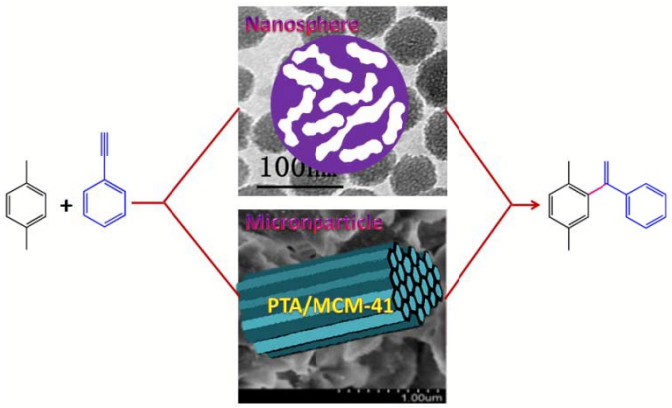

Scheme 2. Schematic for improved catalytic performance in alkenylation of *p*-xylene and phenylacetylene over the PTA/MSN in comparison with traditional PTA/MCM-41 through intensifying mass transfer.

Table 5 Reaction rate for the model reactions over the diverse solid acid catalysts.

Catalyst	Reaction rate (mmol h^{-1} g^{-1}cat)		
	Esterification[a]	Alkylation[b]	Benzylation[c]
PTA/MSN-0.025	19.9	20.5	11.0
PTA/MCM-41	16.4	17.3	8.9
HY	8.2	10.5	4.3
Amberlyst-15	2.8	2.4	2.1
Blank	0.8	0.3	0.2

[a] Reaction condition: acetic acid 128 mmol, ethanol 1mol, catalyst 50 mg, T_r=70 °C, t=5 h. [b] Reaction condition: styrene 128 mmol, benzene 500 mmol, catalyst 50 mg, Tr=70 °C, t=5 h. [c] Reaction condition: benzyl alcohol 50 mmol, benzene 625 mmol, catalyst 200 mg, T_r=110 °C, t=5 h.

properties of different solid acid catalysts for the other diverse transformations including esterification, alkylation, and benzylation were examined. Table 5 summaries the reaction rate for these reactions over PTA/MSN-0.025, PTA/MCM-41, HY, and Amberlyst-15, as well as the blank experiment was also included for comparison. From Table 5, the PTA/MSN-0.025 solid acid catalyst demonstrates much higher reaction rate for the involved reactions in comparison with the other solid acid catalysts. The developed PTA/MSN-0.025 could be considered as a promising solid acid catalyst for diverse transformations.

Conclusions

In summary, In conclusion, this work has presented a facile, low-cost, and scalable templating hydrothermal method for synthesizing monodisperse mesoporous silica nanospheres with tunable particle size and pore structure using CTAB as templating surfactant and urea as mineralizing agent. The particle size and pore structure are strongly dependent on the molar ratio of urea to TEOS. This novel technique has practical applications in industry. By employing MSNs as support, the advanced solid acid catalyst can be synthesized. Besides higher activity, the supported PTA catalyst on MSN-0.025 presents much superior coke-resistent catalytic stability for alkenylation of aromatic with alkyne, a model reaction, in comparison with PTA/MCM-41. This shows that the shortening length of mesopores of solid acid catalysts can be considered as a sapiential strategy for improving catalytic stability through suppressing coke deposition, which presents a practical approach for solving the bottleneck problems of solid acid catalysts. The PTA/MSN-0.025 solid acid catalyst demonstrates outstanding catalytic performance for diverse transformations.

Acknowledgments

This work is financially supported by the National Natural Science Foundation of China (grant no. 21276041, U1261104 and 20803006), also by the Chinese Ministry of Education via the Program for New Century Excellent Talents in Universities (grant no. NCET-12-0079) and the Natural Science Foundation of Liaoning Province (grant no. 2015020200), and the Fundamental Research Funds for the Central Universities (grant no. DUT15LK41), and the Science and Technology Development Program of Hangzhou (20130533B14).

Notes and references

State Key Laboratory of Fine Chemicals, Department of Catalysis Chemistry and Engineering, School of Chemical Engineering, Dalian University of Technology, Dalian 116024, P.R. China. E-mail: zkzhao@dlut.edu.cn; Fax:+86-411-84986354

† Electronic Supplementary Information (ESI) available: Particle size distribution of MSN-*x* NH_3-TPD profiles, extra N_2 physisorption results, low-angle XRD patterns, XRD, and extra reaction results. See DOI: 10.1039/c0ra00000x/

1 a) P. Yang, D. Zhao, D. I. Margolese, B. F. Chmelka, G. D. Stucky, Nature 1998, 396, 152-155; b) V. Alfredsson, H. Wennerstroem, Acc. Chem. Res. 2015, 48, 1891-1900; c) T. Suteewong, H. Sai, R. Hovden, D. Muller, M. S. Bradbury, S. M. Gruner, U. Wiesner, Science 2013, 340, 337-341; d) D. Zhao, J. Feng, Q. Huo, N. Melosh, G. H. Frederickson, B. F. Chmelka, G. D. Stucky, Science 1998, 279, 548-552; e) Y. Wan, D. Zhao, Chem. Rev. 2007, 107, 2821-2860; f) H. Y. Hsueh,C. T. Yao, R. M. Ho, Chem. Soc. Rev. 2015, 44, 1974-2018; g) Y. Wang, H. Gu, Adv. Mater. 2015, 27, 576-585; h) K. Nakajima, M. Okamura, J. N. Kondo, K. Domen, T. Tatsumi, S. Hayashi, M. Hara, Chem. Mater. 2009, 21, 186-193; i) J. Kim, B. Kim, C. Anand, A. Mano, J. S. M. Zaidi, K. Ariga, J. You, A. Vinu, E. Kim, Angew. Chem., Int. Ed. 2015, 54, 8407-8410.

2 a) M. Vallet-Regí, F. Balas, D. Arcos, D. Angew. Chem., Int. Ed. 2007, 46, 7548-7558; b) D. Radu, C. Lai, K. Jeftinija, E. Rowe, S. Jeftinija, V. Lin, J. Am. Chem. Soc. 2004, 126, 13216-13217; c) W. H. Fu, Y. Guan, Y. M. Wang, M. Y. He, Micropor. Mesopor. Mater. 2016, 220, 168-174; d) G. Lai, H. Zhang, A. Yu, H. Ju, Biosensors Bioelectronics 2015, 74, 660-665; e) G. Z. Jin, M. Eltohamy, H. W. Kim, RSC Adv. 2015, 5, 26832-26842; f) S. Ravi, M. Selvaraj, H. Park, H. H. Chun, C. S. Ha, New J. Chem. 2014, 38, 3899-3906; g) J. Wei, Y. Liu, J. Chen, Y. Li, Q. Yue, G. Pan, Y. Yu, Y. Deng, D. Zhao, Adv. Mater. 2014, 26, 1782-1787; h) J. Peng, Y. Yao, X. Zhang, C. Li, Q. Yang, Chem. Commun. 2014, 50, 10830-10833; i) N. Fellenz, P. Martin, S. Marchetti, F. Bengoa, J. Porous Mater. 2015, 22, 729-738.

3 a) K. Suzuki, K. Ikari, H. Imai, J. Am. Chem. Soc. 2004, 126, 462-463; b) A. J. Paula, L. A. Montoro, A. G. Fiiho, O.L. Alves, Chem. Commun. 2012, 48, 591-593; c) C. E. Fowler, D. Khushalani, B. Lebeau, S. Mann, Adv. Mater. 2001, 13, 649-652; d) S. Sadasivan, C. E. Fowler, D. Khushalani, S. Mann, Angew. Chem., Int. Ed. 2002, 41, 2151-2153; e) Y. S. Lin, N. Abadeer, K. R. Hurly, C. L. Haynes, J. Am. Chem. Soc. 2011, 133, 20444-20457; f) M. J. Hollamby, D. Borisova, P. Brown, J. Eastoe, I. Grillo, D. Shchukin, Langmuir 2012, 28, 4425-4433.

4 a) K. Möller, J. Kobler, T. Bein, Adv. Funct. Mater. 2007, 17, 605-612; b) C. Urata, Y. Aoyama, A. Tonegawa, Y. Yamauchi, K. Kuroda, Chem. Commun. 2009, 45, 5094-5096; c) K. Zhang, Y. Zhang, Q. W. Hou, E. H. Yuan, J. G. Jiang, B. Albela, M. Y. He, L. Bonneviot, Micropor. Mesopor. Mater. 2011, 143, 401-405.

5 W. Zhao, H. Zhang, S. Chang, J. Gu, Y. Li, L. Li, J. Shi, RSC Adv. 2012, 2, 5105-5107.

6 a) C. B. Gao, S. A. Che, Adv. Funct. Mater. 2010, 20, 2750-2768; b) V. Cauda, A. Schlossbauer, J. Kecht, A. Zürner, T. Bein, J. Am. Chem. Soc. 2009, 131, 11361-11370; c) S. Huh, J. W. Wiench, B. G. Trewyn, S. Song, M. Pruski, V. S. Y. Lin, Chem. Commun. 2003, 39, 2364-2365.

7 J. Pang, X. Li, G. Zhou, B. Sun, Y. Wei, RSC Adv. 2015, 5, 6599-6606.

8 8 K. Zhang, L. Xu, J. Jiang, N. Calin, K. Lam, S. Zhang, H. Wu, G. Wu, B. Albela, L. Bonneviot, P. Wu, J. Am. Chem. Soc. 2013, 135, 2427-243.

9 Q. Cai, Z. S. Luo, W. Q. Pang, Y. W. Fan, X. H. Chen, F. Z. Cui, Chem. Mater. 2001, 13, 258-263

10 a) Z. K. Zhao, Y. T. Dai, T. Bao, R. Z. Li, G. R. Wang, J. Catal. 2012, 288, 44-53; b) Z. K. Zhao, R. H. Jin, X. L. Lin, G. R. Wang, Energy Sources Part A 2013, 35, 1761-1769.

11 a) T. Nakamura, M. Mizutani, H. Nozaki, N. Suzuki, K. Yano, J. Phys. Chem. C 2007, 111, 1093-1128; b) H. Lin, C. Mou, Acc. Chem. Res. 2002, 35, 927-935.

12 Y. Lin, C. Tsai, Y. Huang, C. Kuo, Y. Hung, D. Huang, Y. Chen, C. Mou, Chem. Mater. 2005, 17, 4570-4573.

13 Y. Shi, Y. Wan, R. Liu, B. Tu, D. Zhao, J. Am. Chem. Soc. 2007, 129, 9522-9531.

14 Z. K. Zhao, Y. T. Dai, J. H.Lin, G. R. Wang, Chem. Mater. 2014, 26, 3151-3161.

15 a) A. Bordoloi, S. Sahoo, N. Lucas, S. B. Halligudi, Adv. Porous Mater. 2013, 1, 255-261; b) D. P. Sawant, A. Vinu, F. Lefebvre, S. B. Halligudi, J. Mol. Catal. A: Chem. 2007, 262, 98-108; c) P. Kamala, A. Pandurangan, Catal. Commun. 2008, 9, 2231-2235; d) Y. Guo, K. Li, J, H. Clark, Green Chem. 2007, 9, 839-841; e) B. C. Gagea, Y. Lorgouilloux, Y. Altintas, P.A. Jacobs, J.A. Martens, J. Catal. 2009, 265, 99-108; f) G. Nie, J. J. Zou, R. Feng, X. Zhang, L.Wang, Catal. Today 2014, 234, 271-277; g) T. H. Kang, J. H. Choi, Y. Bang, J. Yoo, J. H. Song,W. Joe, J. S. Choi, I. K. Song, J. Mol. Catal. A: Chem. 2015, 396, 282-289.

16 T. Yokoi, J.Wakabayashi, Y. Otsuka, W. Fan, M. Iwama, R. Watanabe, K. Aramaki, A. Shimojima, T. Tatsumi, T. Okubo, Chem. Mater. 2009, 21, 3719-3729.

17 a) G. Busca, Chem. Rev. 2007, 107, 5366-5410; b) G. Sartori, R. Maggi, Chem. Rev. 2006, 106, 1077-1104; c) M. H. Chavez-Sifontes, M. E. Domine, S. Valencia, Catal. Today 2015, 257, 305-317; d) J. E. Bruno, K. M. Dooley, Appl. Catal. A: Gen. 2015, 497, 176-183; e) J. Huang, Y. Jiang, V. R. R. Marthala, A. Bressel, J. Frey, M. Hunger, J. Catal. 2009, 263, 277-283.

18 a) Z. K. Zhao, X. H. Wang, Appl. Catal. A: Gen. 2015, 503, 103-110; b) Z. K. Zhao, J. F. Ran, App. Catal. A: Gen. 2015, 503, 77-83.

19 a) Y. Shu, A. Travert, R. Schiller, M. Ziebarth, R. Wormsbecher, W. C. Cheng, Top. Catal. 2015, 58, 334-342; b) Z. Zhao, W. Qiao, X. Wang, G. Wang, Z. Li, L. Cheng, Micropor. Mesopor. Mater. 2006, 94, 105-112; c) Z. Zhao, W. Qiao, G. Wang, Z. Li, L. Cheng, J. Mol. Catal. A: Chem. 2006, 250, 50-56; d) F. J. Maldonado-Hodar, M. F. Ribeiro, J. M. Silva, A. P. Antunes, F. R. Ribeiro, J. Catal. 1998, 178, 1-13.

20 a) A. Corma, Chem. Rev. 1997, 97, 2373-2419; b) S. T. Yang, J. Y. Kim, H. J. Chae, M. Kim, S. Y. Jeong, W. S. Ahn, Mater. Res. Bull. 2012, 47, 3888-3892.

21 a) D. Gao, A. Duan, X. Zhang, K. Chi, Z. Zhao, J. Li, Y. Qin, X. Wang, C. Xu, J. Mater. Chem. A 2015, 3, 16501-16512; b) F. Carniato, C. Bisio, G. Paul, G. Gatti, L. Bertinetti, S. Colucciab, L.Marchese, J. Mater. Chem. 2010, 20, 5504-5509; c) M. Choi, H. S. Cho, R. Srivastava, C. Venkatesan, D. H. Choi, R. Ryoo, Nat. Mater. 2006, 5, 718-723.

22 a) Q. Hou, B. Zheng, C. Bi, J. Luan, Z. Zhao, H. Guo, G. Wang, Z. Li, J. Catal. 2009, 268, 376-383; b) G. Sartori, R. Maggi, Chem. Rev. 2011, 111, PR181-PR214.

Facile, low-cost, and scalable fabrication of particle size and pore structure tuneable monodisperse mesoporous silica nanospheres as supports for advanced solid acid catalysts†

Zhongkui Zhao*[a], Xianhui Wang[a], Yanhua Jiao[b], Boyuan Miao[a], Xinwen Guo[a] and Guiru Wang[a]

[a] State Key Laboratory of Fine Chemicals, Department of Catalysis Chemistry and Engineering, School of Chemical Engineering, Dalian University of Technology, Dalian 116024, P.R. China. E-mail: zkzhao@dlut.edu.cn; Fax:+86-411-84986354.

[b] College of Material Chemistry and Chemical Engineering, Hangzhou Normal University, Hangzhou 310036, P. R. China.

This work presents a facile, low-cost, and scalable strategy for fabricating monodisperse mesoporous silica nanospheres (MSN) with tuneable particle size and pore structure. The high volume efficiency by using high TEOS concentration as Si sources and the low production cost by using urea as mineralizing agent allow it to have great potential for industrial production. Using MSN as a promising support, the advanced solid acid catalysts with much superior catalytic activity and stability were prepared, presenting an alternative method for overcoming low stability issue, a bottleneck problem for the industrial application of solid acid catalysts.